Evidence of the different effect of mercury and cadmium on the hIAPP aggregation process

Daniela Meleleo[1], Andrea Gerbino[1], Maria Mastrodonato[2]

[1] Department of Biosciences, Biotechnologies and Biopharmaceutics, [2] Department of Biology, University of Bari "Aldo Moro", via E. Orabona 4, 70126 Bari, Italy

Running title: Mercury and Cadmium affect differently the aggregation process of hIAPP

Please send all correspondence to: Daniela Meleleo, via E. Orabona 4, 70126 Bari Italy, Tel: +390805442775, E-mail: danielaaddolorata.meleleo@uniba.it

E-mail addresses: andrea.gerbino@uniba.it (A. Gerbino), maria.mastrodonato@uniba.it (M. Mastrodonato)

Abstract

hIAPP is a hormone consisting of 37 aminoacids that shows a strong tendency to self-assemble into β-sheet-rich aggregates, which evolve to form insoluble aggregates that seem to be associated with β-cell degeneration in Type 2 Diabetes Mellitus. Numerous factors, intrinsic and extrinsic to the peptide molecule, appear to influence the hIAPP aggregation process. Different metal ions are able to interact with the hIAPP molecule, modulating its secondary structure and subsequently the peptide's capacity to aggregate. In this study, the effect of Hg^{2+} and Cd^{2+} on the hIAPP aggregation process was evaluated using direct and indirect methods. The kinetics and morphology of amyloid aggregate formation were respectively evaluated with Thioflavin T assays and electron microscopy, while the ability of the peptide to incorporate into POPC PLMs and form ion channels was monitored by single-channel current measurements. Hg^{2+} and Cd^{2+} each seem to modulate the peptide's ability to aggregate in a different way, suggesting a different mechanism of hIAPP toxicity.

Keywords: hIAPP, Mercury, Cadmium, Toxicity, Ion channel

1. Introduction

Human Islet amyloid polypeptide (hIAPP), or amylin, is a protein hormone synthesized and secreted into the blood together with insulin by the pancreatic islet β-cells. It regulates and maintains blood glucose levels in the body and its effects are complementary to those of insulin (1, 2). The physiological functions of hIAPP as a hormone are to slow down gastric emptying, to suppress food intake and to control glucose homeostasis (3, 4).

hIAPP is a hormone consisting of 37 aminoacids in its native form with a molecular weight of 3.9 kDa. It has an amidated C-terminus and a disulfide bridge between Cys-2 and Cys-7; the N-terminus of IAPP resembles a sequence in the calcitonin polypeptide family (5). Like the components of the calcitonin polypeptide family, hIAPP also shows a strong tendency to self-assemble into β-sheet-rich aggregates, which evolve to form insoluble fibrils that seem to be associated with β-cell degeneration in Type 2 Diabetes Mellitus (T2DM) which is classified as an amyloid disease (6). Furthermore, recent studies show that IAPP is able to heteropolymerize with other proteins. An example is the $hIAPP_{37}$-Aβ42 hetero-complex which represents a link between Alzheimer's disorder and T2DM (7).The relationship between the process of hIAPP aggregation and the onset of T2DM is not entirely understood (8). In a recent review, Milardi and colleagues discuss current knowledge of the structures and pathology associated with hIAPP self-assembly in order to identify therapeutic opportunities (9). However, histological sections from T2DM patients have shown a positive correlation between amyloid aggregates and the reduction in β-cell mass in pancreatic islets (10). Moreover, the missense S20G mutation in the IAPP gene has been identified in the Japanese population and is associated with early onset and severity of T2DM (11). Several studies suggest that transient and heterogeneous hIAPP oligomers are more toxic to β-cells than monomers and fibrils, and their structures have been determined by different techniques. Linear fibrils and annular aggregates have been determined by solid-state NMR and AFM respectively, while linear, annular and triangular structures have been predicted by molecular simulations (12-16). The main target of hIAPP aggregates seems to be the plasma membrane, whose disruption can occur via different mechanisms. hIAPP can interact with various membrane receptors such as CT, RAMPs receptor (17, 18) and amylin receptor (19). hIAPP oligomers can interact directly with the membrane, either by forming ion channels or in a detergent-like mode producing an uncontrolled influx of ions into the cell (16, 20). Although the molecular mechanisms of hIAPP-membrane interaction and subsequent membrane damage remain poorly understood, numerous studies have been conducted in an attempt to elucidate the interactions of hIAPP monomers, oligomers, protofibrils with the lipid bilayer (21-28).

The hIAPP aggregation process seems to depend both on intrinsic factors of the peptide (concentration, electrostatic and/or hydrophobic interactions) and on extrinsic factors such as pH (29,

30), temperature (31, 32) and metal ions (33, 34). The hIAPP aggregation rate depends on its concentration, which is related with cytotoxicity. The study carried out on two different cell lines (Rat insulinoma INS-1 cells and COS-1 cells) by Magzoub and colleagues (35) shows that the cytotoxic concentration of hIAPP is in the range of 5-25 μM, given that it induces a percentage of dead cells ranging from 15 to 80%, respectively. A possible mechanism of action underlying its toxicity lies in the property of His18 to act as an electrostatic switch, which, depending on its state of charge, can promote or slow down the aggregation process. Some authors have reported that His18 inhibits aggregation when it is in a charged state that is pH-dependent (29, 36). Recently, the role of metal ions in the hIAPP aggregation process has been investigated. Brender and colleagues (33) showed that zinc ions (Zn^{2+}) bind to the His18 residue of monomeric amylin, while the results of another study show that Zn^{2+} coordinated with 4 amino acids of a protein to form a tetrahedral coordination complex with it (37). Ramamoorthy's group has extensively studied the effect of Zn^{2+} on the hIAPP aggregation process (38, 39). A similar effect to Zn^{2+} has also been observed for aluminum ions (Al^{3+}) which at a concentration of 10 μM promote the formation of protofibril oligomers that evolve into fibrils (40, 41). However, the effect of Zn^{2+} ions on the amyloid aggregation process of IAPP appears to depend on the physiological environment of the β cell granules. The β cell granules contain IAPP, high concentrations of Zn^{2+}, insulin and C-peptide. Ge and collaborators showed that a Zn^{2+} ion coordinates a heterotrimer with a C-peptide molecule and two IAPP molecules which makes the amyloidogenic region of IAPP less prone to aggregate (42). On the other hand, some authors (43) have shown that the copper ion (Cu^{2+}) inhibits fibril formation by modulating the arrangement of amylin dimers and binding preferentially to the β-hairpin fragment of the amylin monomer. Cu^{2+} ions seem to stabilize hIAPP in its native, non-toxic random coil conformation as found by different groups of researchers (44, 45). Sinopoli and colleagues studied hIAPP conformation in the absence and presence of Cu^{2+}. The authors conclude that there are no clear signs of β-sheet conformation, suggesting that hIAPP fibril formation can be inhibited by the metal ion (46). Mukherjee et al. found that iron ions (Fe^{2+}), in the form of heme, are able to bind to two molecules of hIAPP (47). The results of these studies seem to indicate that Zn^{2+}, Al^{3+} and Fe^{2+} promote the formation of hIAPP oligomers/protofibrils, while Cu^{2+} ions can inhibit amylin fibrillation.

The effects of other metal ions on the hIAPP fibrillation process, such as gold ions (Au^{3+}), ruthenium (Ru) complexes and vanadium ions (V), have been studied. The results show that Ru complexes (48-51), V complexes (52, 53) and some of the Au^{3+} complexes (54) inhibit the fibrillation process and oligomer/protofibril formation. Nevertheless, for Au^{3+} complexes, the nature of their effect on fibril formation depends on concentration.

In recent years, numerous studies have shown a link between glucose metabolism, T2DM risk and exposure to mercury and cadmium, two environmental pollutants known for their toxicity. Epidemiological studies conducted on a sample of the Chinese (55, 56), Pakistan (57, 58), American (59, 60) and Australian (61) populations show a significant correlation between cadmium exposure and fasting blood glucose levels resulting in the development of T2DM. This is confirmed by the results of a study conducted on a lead smelter community. T2DM development in subjects under the age of 50 was associated with cadmium exposure, but not in subjects over the age of 50. These results suggest that cadmium exposure increases the propensity to insulin resistance and the risk of T2DM (62). Similar results have been reported for mercury exposure (63, 64). He and colleagues conducted a study on a sample of young American adults exposed to mercury and found that young people exposed to higher levels of mercury have a higher risk of developing T2DM (65). The results of the study conducted by Cordier and colleagues on two Canadian indigenous populations (66) and by Jeppensen and colleagues on the Inuit population of Greenland (67) show that mercury exposure increases fasting blood glucose levels.

The mechanisms by which the two heavy metals affect blood glucose levels have not been fully understood. Studies in animal models indicate that the two metals accumulate in the pancreas, altering the functions of the pancreatic islet cells and contributing to dysglycemia. Cadmium accumulates in β-cells by altering insulin secretion (68, 69). Other studies indicate that cadmium may act on some glucose transporters, thus affecting blood glucose levels (70). Mercury induces pancreatic islet cell dysfunction and apoptosis that are caused by oxidative stress from ROS production (71-73). Exposure to mercury, as well as to other toxic chemicals, can lead to ROS production (74, 75). Therefore, mercury could indirectly contribute to T2DM pathology. Another mechanism proposed to explain mercury's toxic effect on β cells involves mitochondrial dysfunction. Mercury compounds decrease ATP production (76); the pancreatic β cells of diabetic patients show reduced ATP synthesis, which can affect insulin secretion (77). Therefore mercury could exacerbate the reduced ATP synthesis of diabetic patients' β cells.

On the other hand, some studies report no significant relationship between mercury and cadmium exposure and the development of diabetes (78-82).

In this paper, we hypothesize that mercury and cadmium (used in the form of inorganic cations, Hg^{2+} and Cd^{2+}, respectively) can influence the hIAPP aggregation process by modulating the formation of aggregates and/or fibrils which in turn appear to be responsible for the toxicity of the peptide. We carried out experiments with: - the electrophysiological technique of single-channel current measurements to evaluate the ability of the hIAPP peptide, pre-incubated with Hg^{2+} and Cd^{2+}, to incorporate into planar lipid membranes (PLMs) made of Palmitoyl-oleoyl-phosphatidylcholine

(POPC); - the fluorescence technique using the fluorophore thioflavin T (ThT) to monitor the kinetics of hIAPP amyloid aggregate formation in the absence and in the presence of two metal ions; - the transmission electron microscopy (TEM) technique to directly evaluate the effect of the two metal ions on hIAPP molecule morphology.

2. Materials and Methods

2.1. Chemicals

Cadmium chloride ($CdCl_2$), Mercury chloride ($HgCl_2$), Potassium chloride (KCl), ThT, and 1,1,1,3,3,3-hexafluoro-2-propanol (HFIP), n-Decane were purchased from Sigma (Germany), Palmitoyl-oleoyl-phosphatidylcholine (POPC) was purchased from Avanti Polar Lipid (Alabaster, AL). Amylin or hIAPP was purchased from Sigma (Germany) and from Alexotech (Sweden).

2.2. Preparation of hIAPP and heavy metals solutions

For the single-channel measurement experiments, a stock solution of hIAPP (Sigma) was prepared by dissolving hIAPP powder (0.1 mg) in 100 µL of bidistilled sterile water under stirring for 5 min to obtain a concentration of 256 µM. From this solution, 5 µL were withdrawn and diluted in 45 µL of bidistilled sterile water under stirring for 5 min to obtain a concentration of 25.6 µM. The solutions were stored at -20°C until use. Stock solutions of $CdCl_2$ or $HgCl_2$ were prepared by dissolving $CdCl_2$ or $HgCl_2$ powder (4.6 and 5.4 mg, respectively) in 10 mL of bidistilled sterile water under stirring for 10 min to obtain a concentration of 2 mM. The $CdCl_2$ or $HgCl_2$ solutions at concentrations of 0.2 mM were obtained from stock solution by scalar dilution. The solutions of the two different salts were stored at 4°C until use.

For the TEM and ThT experiments, 1 mg of hIAPP (Alexotech) was dissolved in HFIP and incubated at Room Temperature (RT) for 6 hours. Then, the solution was divided into equal portions and all aliquots were frozen at -80°C for 24 hours and lyophilized overnight. The lyophilized samples were stored at -20°C until use. This protocol was used to obtain a disaggregated peptide. The lyophilized samples were solubilized in phosphate-buffered saline (PBS 50 mM pH 7.4) to a concentration of 33 µM/10 µM just before the TEM and ThT measurements, respectively. Stock solutions of $CdCl_2$ or $HgCl_2$ were prepared by dissolving $CdCl_2$ or $HgCl_2$ powder (11.4 and 13.6 mg, respectively) in 5 mL of bidistilled sterile water under stirring for 10 min to obtain a concentration of 10 mM. The $CdCl_2$ or $HgCl_2$ solutions at concentrations of 5 and 1 mM were obtained from stock solution by scalar dilution. The solutions of the two different salts were stored at 4°C until use.

2.3. Single-channel measurement

hIAPP incorporation and channel formation were studied in PLMs made of POPC in 1% n-decane , prepared as previously described (83-85).

The methodology and the experimental set-up used for single-channel measurements are the same as those reported in our previous studies (86, 87). Briefly, PLMs were formed across a 300 μm hole in a Teflon partition separating two Teflon chambers (volume 4000 μL) which held symmetrical 0.1M KCl solutions, pH=7, temperature 23±1°C. The aqueous solutions were used unbuffered. The salts used in the experiments were of analytical grade. The Müller-Rudin or painted technique (88-90) was used to form PLMs. The membrane current was monitored using the experimental set-up described by Gallucci et al. (91) and Stipani et al. (92) and recorded on a chart recorder for further analysis by hand. Membrane capacitance was calculated using a calibration curve as described by Micelli et al. (93). The single-channel data, filtered at 300Hz as reported by other authors (94) were obtained from at least four experiments performed on different days.

To evaluate hIAPP's ability to incorporate and form ion channels in POPC PLMs, we carried out experiments in which 15.60 μL of hIAPP solution at a concentration of 25.6 μM was added to the *cis* side of the membrane to obtain the final hIAPP concentration of 0.1 μM.

To monitor the effect of Hg^{2+} or Cd^{2+} on the peptide in solution, the following experimental sets were prepared:

- in the first experimental set, 2.16 μL of $HgCl_2$ or $CdCl_2$ (0.2 mM) was added to 16.80 μL of hIAPP (25.6 μM). The molar ratio hIAPP:Hg^{2+} or Cd^{2+} was 1:1, respectively;
- in the second experimental set, 1.10 μL of $HgCl_2$ or $CdCl_2$ (2 mM) was added to 16.90 μL of hIAPP (25.6 μM). The molar ratio hIAPP:Hg^{2+} or Cd^{2+} was 1:5, respectively.

After preparation, each metal ion-peptide mixture was stirred for 3 min. For each experimental set, hIAPP was pre-incubated with metal ions for incubation times of 24 hours at RT. Once the bilayer was formed, 17.60 or 16.60 μL of the first or second mixture, carefully stirred for 3 min, was added to the *cis* side of the membrane to obtain the final hIAPP concentration of 0.1 μM and the following metal ion concentrations:

- in the first experimental set, 0.1 μM of $HgCl_2$ or $CdCl_2$;
- in the second experimental set, 0.5 μM of $HgCl_2$ or $CdCl_2$.

In all experiments, before the addition of known volumes of hIAPP solution or metal ion-peptide mixture, membrane stability was tested by applying voltages of ±40, ±80 and ±100 mV for 5-6 minutes each and measuring constant values of conductance and capacitance.

The biophysical and statistical parameters considered to evaluate hIAPP incorporation either alone or pre-incubated with different concentrations of metal ions were single-channel conductance,

channel size and frequency. To determine conductance, a histogram of the conductance amplitude distribution for each experimental set was constructed and fitted by a Gaussian distribution function. Results are expressed as central conductance ± standard error (Λ_c ± SE) and were evaluated by analysis of variance (ANOVA-Tukey test).

To determine the frequency (number of channels in 60 s), any detection of channel events was counted as successful. Results are expressed as frequency ± standard deviation (F ± SD).

To calculate the size of the hIAPP channel, the following formula was used:

$$1) \qquad \Lambda_c = \frac{(\sigma \times \pi \times r^2)}{d}$$

where Λ_c is the central conductance, σ is the specific conductibility of the solution filling the channel, π has the value of 3.14, r is the channel radius and d is the channel length.

2.4. Thioflavin-T assay

ThT is a fluorescent dye used for biophysical studies of protein aggregation to investigate amyloid formation. To perform the fluorescence study, a stock solution of ThT in PBS (50 mM, pH=7.4) at a concentration of 5 mM was used. To monitor hIAPP amyloid aggregate formation and the effect of different concentrations of Hg^{2+} or Cd^{2+}, the following samples were prepared:

-in the hIAPP sample, 210 µL of stock solution of hIAPP (10 µM) were mixed with 2.1 µL of ThT (5 mM);

-in the hIAPP+Hg^{2+} or Cd^{2+} (10 µM) samples, 210 µL of stock solution of hIAPP (10 µM) were mixed with 2.1 µL of $HgCl_2$ or $CdCl_2$ (1mM) and 2.1 µL of ThT (5 mM). The molar ratio hIAPP:Hg^{2+} or Cd^{2+} was 1:1, respectively;

- in the hIAPP+Hg^{2+} or Cd^{2+} (50 µM) samples, 210 µL of stock solution of hIAPP (10 µM) were mixed with 2.1 µL of $HgCl_2$ or $CdCl_2$ (5mM) and 2.1 µL of ThT (5 mM). The molar ratio hIAPP:Hg^{2+} or Cd^{2+} was 1:5, respectively;

- in the control samples, 210 µL of PBS were mixed with 2.1 µL of $HgCl_2$ or $CdCl_2$ (1, 5 mM depending on the corresponding sample) and 2.1 µL of ThT (5 mM).

In all samples, the final concentrations of hIAPP (except in control samples) and ThT were 10 µM and 50 µM, respectively.

ThT fluorescence was monitored as a function of time in a 96-well black plate with clear bottom using a TECAN plate reader (TECAN Infinite M1000 pro, Switzerland), temperature 25°C, pH=7.4. The samples were shaken orbitally for 30 s, with an amplitude of 6 mm and a frequency of 120 rpm. Emission was measured at 482 nm and excitation at 450 nm using a slit measuring 5 nm; the time interval between the data points was 30 s. Each experiment was performed in duplicate.

2.5. Fluorescence Microscopy

ThT was used to set up the hIAPP samples analyzed with fluorescence microscopy. Preliminarily, we prepared 50 μM $HgCl_2$ and $CdCl_2$ in PBS, mixing 2.5 μL of $HgCl_2$ or $CdCl_2$ (2 mM aqueous solution) with 97.5 μL of PBS, respectively. The hIAPP samples (10 μM) without and with pre-incubation with Hg^{2+} or Cd^{2+} (50 μM) at RT for 20 min (T0), 24 h (T24) and 72 h (T72) were set up as follows:

- in the hIAPP sample, 3 μL of stock solution of hIAPP (33 μM) were mixed with 4.5 μL of PBS and with 2.5 μL of ThT (0.2 mM). The final concentration of peptide was 10 μM;
- in the hIAPP+Hg^{2+} or Cd^{2+} (50 μM) samples, 3 μL of stock solution of hIAPP (33 μM) were mixed with 4.5 μL of $HgCl_2$ or $CdCl_2$ (50 μM) in PBS and with 2.5 μL of ThT (0.2 mM). The hIAPP:Hg^{2+} or Cd^{2+} molar ratio was 1:5 in both cases.

The ThT solution in PBS at a concentration of 0.2 mM was prepared extemporaneously and added to the Eppendorf containing the samples 15 minutes before instrumental analysis. A drop of sample (7 μL) was placed on a microscope slide, covered with a coverslip and mounted on the stage of a Leica DM6000 B Motorized Fluorescence Phase Contrast Microscope. ThT samples were illuminated through a 10× or 40× lens at 480/40 nm. The emitted fluorescence was passed through a dichroic mirror, filtered at 527/30 nm, and captured by a Leica DFC 310 FX digital color camera.

2.6. Transmission Electron Microscopy

The morphology of hIAPP aggregates, in the absence and presence of Hg^{2+} or Cd^{2+}, was evaluated by TEM. hIAPP (10 μM) was incubated either alone or with 10, 50 μM $HgCl_2$ or $CdCl_2$ at RT for 20 min (T0), 24 h (T24) and 72 h (T72).

Preliminarily, we prepared 10 and 50 μM $HgCl_2$ and $CdCl_2$ in PBS, mixing 2.5 μL of $HgCl_2$ or $CdCl_2$ (2 mM aqueous solution) with 497.5 and 97.5 μL of PBS, respectively. The samples were prepared as follows:

-in the hIAPP sample, 3 μL of stock solution of hIAPP (33 μM) were mixed with 7 μL of PBS, obtaining a final concentration of 10 μM;
-in the hIAPP+Hg^{2+} or Cd^{2+} (10 μM) samples, 3 μL of stock solution of hIAPP (33 μM) were mixed with 7 μL of $HgCl_2$ or $CdCl_2$ (10 μM) in PBS, obtaining a hIAPP:Hg^{2+} or Cd^{2+} molar ratio of 1:1 in both cases;
- in the hIAPP+Hg^{2+} or Cd^{2+} (50 μM) samples, 3 μL of stock solution of hIAPP (33 μM) were mixed with 7 μL of $HgCl_2$ or $CdCl_2$ (50 μM) in PBS, obtaining a hIAPP:Hg^{2+} or Cd^{2+} molar ratio of 1:5 in both cases.

Then, 10 μL of each sample were blotted on a carbon-coated Formvar 300 mesh copper grid for 1 min. Excess sample was removed with filter paper and grids were washed. Grids were negatively stained with saturated uranyl acetate for 1 min, dried at room temperature, and then observed under a Morgagni 268 electron microscope (FEI, Hillsboro, Oregon, USA) with a voltage of 70 kV.

3. Results

3.1. hIAPP incorporation and channel formation in POPC PLMs

In all experiments, before the addition of peptide solution, the capacitance and conductance of membrane were monitored at applied voltages of ±40, ±80 and ±100 mV; the voltage was applied for 5-6 min at 40 mV followed by 5-6 min at -40 mV and so on. PLMs were stable and no channel activity was present. After this phase of membrane stabilization, 15.60 μL of hIAPP at the concentration of 25.6 μM was added to the *cis* side of membrane at an applied voltage of 100 mV (addition voltage). The channel activity of hIAPP appears after about 120 minutes' lag time at an applied voltage of 100 mV (activation voltage) as discrete non-random current fluctuations, compatible with channel-type openings and closures. Current fluctuations show different conductance levels that alternate with quiescence periods. After the first channel formation, the applied voltage was lowered as far as ±20 mV and channel amplitude was monitored. hIAPP channel activity was recorded in the voltage range of ±20 to ±100 mV; each voltage was applied for 60 min starting from 100 mV (i.e. 60 min at 100 mV, followed by 60 min at -100 mV, and so on). Examples of chart recordings of hIAPP channel activity are shown in Figure 1.

For each applied voltage, experimental data of conductance levels were used to construct a histogram of the conductance amplitude distribution that shows that there is one main conductance level at all applied voltages. Histograms constructed at different applied voltages were fitted by a Gaussian distribution function and gave the central value of hIAPP channel conductance (Λ_c).

Λ_c values (Λ_c±SE) as a function of applied voltage are reported in Table 1. It is worth noting that Λ_c seems to be dependent on the applied voltages, decreasing as the voltage is increased. By means of the Λ_c value and assuming that a cylindrical channel with a length (d) of 5 nm (corresponding to the membrane thickness) is filled with a solution of the same specific conductibility (σ) as the external medium, we calculated the hIAPP channel diameter (diameter=2r) that is 5.55 Å at an applied voltage of 60 mV.

Another parameter considered in this study is the frequency of hIAPP channel occurrence. The frequency values (F±SD) seem to be symmetrical for negative and positive applied voltages, indicating that channel turnover is independent of the applied voltage sign (Table 2).

The results obtained from this experimental set show that the hIAPP peptide is able to incorporate into PLMs made up of POPC and to form ion channels.

3.2. Effect of Hg^{2+} and Cd^{2+} different concentrations on hIAPP channel activity

Numerous studies show that different ions (see Introduction) are able to bind to specific aminoacids of hIAPP and to modulate its aggregation. We performed two series of experiments in which hIAPP was pre-incubated for 24 hours with different concentrations of Hg^{2+} and Cd^{2+} and we evaluated hIAPP's capacity to incorporate into PLMs made up of POPC and to form ion channels.

Preliminarily, we performed control experiments to exclude any destabilizing effects of Hg^{2+} or Cd^{2+} on the PLMs by adding $HgCl_2$ or $CdCl_2$ (0.1 and 0.5 μM final concentrations) to the *cis* side of the medium facing the membrane. The membrane conductance and capacitance were monitored for a long period (10-12 hours) at applied voltages of ±80 and ±100 mV, returning constant values of 13 pS and 0.35 $\mu F/cm^2$ respectively, while the PLMs manifested no channel-like activity.

In the peptide pre-incubation experiments with the two metal ions, before the addition of the mixture to the *cis* side of the membrane, the PLMs were stabilized using the same experimental protocol used in the experiments with hIAPP alone, while monitoring constant values of conductance and capacitance.

A known volume of mixture, with either metal ion and at either concentration, was added at an applied voltage of 100 mV (addition voltage) under stirring for 5 min.

3.2.1. hIAPP channel activity pre-incubated with 0.1 μM Hg^{2+} and Cd^{2+}

In the pre-incubation experiments in which the concentration of the two metal ions was 0.1 μM, channel activity appears at an applied voltage of 100mV after a lag time of 90/120 minutes for Hg^{2+}/Cd^{2+}, respectively. Channel activity was monitored in the voltage range of ±60 to ±100 mV, while each applied voltage was applied for 60 min starting from 100 mV using the same experimental procedure as in the experiments with the peptide alone. Channel activity appears as discrete current jumps that fluctuate between open and closed states with different levels of conductance, whose amplitude and frequency can be measured. Besides, at applied voltages of ±100 mV, it is possible to observe quiescence periods that alternate with paroxystic activity periods, during which the number of channels cannot be rigorously analysed. It is important to note that no channel activity appeared in the applied voltages range of ±20 to ±40 mV, even upon successive application of voltages as high as ±120 mV or membrane breakage by the operator and its subsequent reconstitution using the lipid solution present around the hole. Examples of chart recordings of the hIAPP peptide pre-incubated with 0.1 μM Hg^{2+} or Cd^{2+} are shown in Figure 1.

To determine the central conductance values, the experimental data were fitted with a Gaussian distribution function, and when calculating the frequency values any detection of channel events was counted as successful. Λ_c±SE and F±SD values are reported in Tables 1 and 2, respectively. It is worth noting that: - for each metal ion used, the Λ_c values decrease as the voltage is increased and the F values seem to be independent of applied voltages; - the Λ_c values obtained by pre-incubating the peptide with 0.1 μM Hg^{2+} or Cd^{2+} are not significantly different at any of the applied voltages; - the F values obtained from pre-incubation experiments with 0.1 μM Hg^{2+} are significantly higher than those obtained with pre-incubation with Cd^{2+} at the same concentration.

By means of formula 1 and assuming the same values of σ, π and d used previously, we calculated the channel diameter formed by the hIAPP peptide pre-incubated for 24 hours with 0.1 μM Hg^{2+} or Cd^{2+} at an applied voltage of 60 mV. The channel diameter values are 4.62/4.73 Å, respectively.

The results obtained from this experimental set show that: - hIAPP pre-incubated for 24 hours with 0.1 μM Hg^{2+} or Cd^{2+} is able to incorporate into POPC PLMs and to form ion channels whose diameter is significantly smaller than that calculated without pre-incubation; - channel turnover is favoured by pre-incubation of hIAPP with Hg^{2+}, because the F values obtained in the presence of this metal ion are significantly higher than those in the presence of Cd^{2+}, suggesting that the two ions exert different effects on the hIAPP molecule in solution.

3.2.2. hIAPP channel activity pre-incubated with 0.5 μM Hg^{2+} and Cd^{2+}

To evaluate whether the two metal ions have a different effect on the peptide in solution depending on their concentration, we performed a second series of experiments pre-incubating the hIAPP peptide for 24 hours with 0.5 μM $HgCl_2$ or $CdCl_2$. Some channel activity of hIAPP pre-incubated with Hg^{2+} appears after a lag time of 30 minutes and manifests with multiple levels of conductance and different frequencies. The periods of paroxystic activity are more frequent than those observed at a pre-incubation concentration of 0.1 μM. Using the same experimental procedure reported above, we monitored channel activity in the applied voltages range of ±40 to ±100 mV. No channel activity appeared at ±20 mV, even upon successive application of voltages as high as ±120 mV or membrane breakage by the operator. The channel activity of the peptide pre-incubated with 0.5 μM Cd^{2+} was different from that with Hg^{2+}. After a lag time of about 60 min, channel activity appeared at an applied voltage of 100 mV (activation voltage) and was monitored in the range of ±40 to ±100 mV. It is important to note that, two hours after the first channel formation, the frequency of channel occurrence is lower than that obtained by pre-incubating with Hg^{2+} at the same concentration, while the current jumps seem to present a similar amplitude. Even under this experimental condition, we did not find any channel activity at applied voltages of ±20 mV, not even by subsequently applying

voltages as high as ±120 mV. Examples of chart recordings of hIAPP peptide pre-incubated with 0.5 μM Hg^{2+} or Cd^{2+} are shown in Figure 1.

Similarly to the above experiments, the experimental data were fitted with a Gaussian equation, obtaining the Λ_c values reported in Table 1. The Λ_c±SE values obtained in this experimental set (pre-incubation with 0.5 μM Hg^{2+} or Cd^{2+}) are inversely correlated with applied voltage, decreasing as voltage increases, and are not significantly different at all applied voltages.

The F values calculated under the same experimental conditions are reported in Table 2. F±SD values in the presence of 0.5 μM Hg^{2+} are higher at positive than at negative applied voltages, indicating their dependence on applied voltage sign, whereas the F±SD values obtained pre-incubating hIAPP with 0.5 μM Cd^{2+} are symmetrical for negative and positive applied voltages. Besides, it is important to note that the F values obtained by pre-incubating hIAPP with 0.5 μM Hg^{2+} are significantly higher than those obtained through pre-incubation with 0.5 μM Cd^{2+}, indicating that hIAPP channel turnover is favoured by pre-incubation with Hg^{2+}.

As for the other experimental sets, we calculated the diameter of the hIAPP channel after pre-incubation with 0.5 μM of Hg^{2+} and Cd^{2+} using formula 1 and the same values of σ, π and d. The values of the channel diameter are 4.05 and 4.29 Å, respectively, at an applied voltage of 60 mV.

The results of the biophysical parameters of the hIAPP ion channel without and with pre-incubation for 24 hours with Hg^{2+} or Cd^{2+} show that: - irrespective of the pre-incubating concentration of the two metal ions, the inversely proportional relationship between central conductance and applied voltage is conserved and the Λ_c values without pre-incubation are significantly higher than those with pre-incubation (Table 1), indicating that pre-incubation with the two metal ions favoured incorporation and formation of smaller conductive units in the PLM than those formed of the peptide alone; - independently of the pre-incubating concentration of Hg^{2+}, the F values are significantly higher than those obtained without pre-incubation, indicating that more hIAPP molecules in solution are available to incorporate and form ion channels in PLMs; - depending on the pre-incubation concentration of Cd^{2+}, the F values are not significantly different from those obtained with hIAPP alone when the Cd^{2+} concentration is 0.1 μM, while they are significantly lower at a pre-incubating concentration of 0.5 μM, indicating that hIAPP channel turnover depends on Cd^{2+} concentration decreasing as ion concentration increases. At the 0.5 μM pre-incubating concentration, the number of hIAPP molecules in solution available to incorporate and form ion channels seems to be lower than under the other experimental conditions.

These results seem to suggest that each metal ion has a different effect on hIAPP peptide molecules in solution.

3.3. Hg^{2+} and Cd^{2+} have different effects on the formation kinetics and morphology of amyloid aggregates

The results of single-channel experiments show the different effects of Hg^{2+} and Cd^{2+} on hIAPP channel turnover, suggesting that the two ions modulate the aggregation process of peptide differently in solution. The kinetics of hIAPP aggregation process in the absence and in the presence of different concentrations of Hg^{2+} and Cd^{2+} were studied by ThT fluorescence. ThT is a dye used to follow the protein aggregation state and it interacts with β-sheets containing amyloid aggregates. In our experiments, the kinetic growth of amyloid aggregates was followed at 25°C over a period of 7200 s. Figure 2 shows that the fluorescence intensity was increased when the peptide (10 μM) was alone in solution, while, in the presence of Hg^{2+} 10 μM, the intensity was suppressed up to ~84%, indicating that Hg^{2+} inhibits amyloid aggregate formation. However, the decrease in fluorescence intensity could be affected by changes in the fluorescence quantum yield and the binding constant of ThT. By contrast, fluorescence intensity increased by up to ~85% in the presence of Cd^{2+} 10 μM compared with that of hIAPP alone (Fig. 2A). By increasing the concentration of the two metal ions (50 μM), their effect on the kinetics of the hIAPP aggregation process does not change (Fig. 2B), although the decrease in fluorescence intensity was up to 8% in the presence of Hg^{2+} and the increase in intensity was up to 12% in the presence of Cd^{2+}. It is important to note that the percentage values of the fluorescence intensity decrease or increase in a more evident manner when the molar ratio hIAPP: Hg^{2+} or Cd^{2+} is 1:1 compared to when it is 1:5, as shown in Figure 2C.

To confirm the result obtained with fluorescence spectroscopy, we carried out experiments with fluorescence microscopy, which directly permits to observe the aggregates formed upon binding with ThT dye. Figure 3 shows the fluorescence microscopy images of hIAPP (10 μM) in the absence and in the presence of Hg^{2+} or Cd^{2+} (both 50 μM) after 0, 24 and 72 h of incubation. At incubation time 0, few aggregates were detected in all samples. After 24 h, some small aggregates were observed in samples containing Hg^{2+} and Cd^{2+}, whereas few aggregates had emerged in pure hIAPP samples. Incubation for 72 h induced the formation of larger aggregates in pure hIAPP samples, whereas they were more numerous and larger in samples with Cd^{2+}, and hIAPP samples in the presence of Hg^{2+} still showed fewer and smaller aggregates. These results were in good agreement with those obtained by fluorescence spectroscopy.

The results obtained measuring the changes in ThT fluorescence intensity suggest that Cd^{2+} favours amyloid aggregate formation, in line with the frequency values obtained by single-channel measurements.

The morphology of the amyloid aggregates in the absence and in the presence of the two ions was visually probed by TEM.

TEM images of the hIAPP peptide alone (10 μM) show the presence of amyloid aggregates that over time (0 to 72 hours) become larger, more extensive and more electron-dense (Fig. 4 A,B,C). Besides, it is important to note that TEM analysis of the samples at T0 shows short, scattered aggregates, which decrease in the sample at T24 and are almost completely absent after 72 hours of incubation, indicating the coexistence of structures of different sizes. The different effect of Hg^{2+} and Cd^{2+} (equimolar ratio with the peptide) on the morphology of the amyloid aggregates is clearly visible in Figure 4, respectively in images D,E,F and G,H,I,. The amyloid aggregates in the presence of Hg^{2+} are smaller and less electron-dense than those obtained in the presence of Cd^{2+}. Furthermore, in the images at T0 and T24 obtained in the presence of Hg^{2+}, shorter and more scattered structures coexist with larger ones. The different effect of each metal ion is more evident when the incubation concentration of Hg^{2+} and Cd^{2+} is 50 μM (Fig. 4 L,M,N and O,P,Q, respectively). The results obtained with TEM would seem to be in agreement with those obtained using the other techniques described herein.

4. Discussion

hIAPP is a small peptide with a strong tendency to misfold and to aggregate into oligomers, profibrils and fibrils. In its misfolded form, the peptide is highly toxic. The mechanisms of its toxicity have not been fully understood. The first studies, dating back about thirty years, showed that hIAPP cytotoxicity can be attributed to the formation of fibrils which induce pancreatic β-cell apoptosis (95). These observations suggested that amyloid fibrils may act as pathological agents in T2DM. Indeed, Röchen's studies showed a positive correlation between the presence of amyloid aggregates and the reduction in the mass of pancreatic islet β-cells (10). Subsequently, the observation that amyloid deposits were not present in the pancreatic islets of all patients with T2DM, and that they were also present in non-diabetic subjects, suggested that the cytotoxicity of the hIAPP peptide could be attributed to soluble and low-molecular-weight oligomers. The main target of these oligomers seems to be the cell membrane, with which they can interact in different ways, binding to membrane receptors (17-19), causing variations in the thickness or curvature of the membrane, fragmenting the membrane with detergent-like modes or forming ion channels (20, 96). As proposed for other amyloidogenic peptides (97), hIAPP could destroy the membrane by a two-step process, the initial formation of ion-selective pores followed by nonspecific fragmentation of the lipid membrane during amyloid fiber formation. The process appears to be modulated by the lipid composition of the membrane (98) and calcium ions (99-101).

In our work, we initially evaluated the ability of the hIAPP peptide to incorporate and form ion channels in POPC PLMs, the most abundant phospholipids of the outer layer of the cell plasma membrane. The results obtained from the single-channel experiments show that: - hIAPP is able to incorporate and form ion channels in POPC PLMs; - the conductance of the channel appears to be dependent on the applied voltage; - the frequency of occurrence of the channel seems to be independent of the applied voltage. These results are apparently in line with those obtained by other authors. Using model lipid systems, Mirzabekov and collaborators showed that hIAPP is able to form pores in a membrane whose biophysical parameters have been determined (96). Zhao and collaborators investigated the interactions of hIAPP with the membrane, the ion conductivity and the dynamic structure of the channels formed by the peptide in DOPC membranes by means of molecular modelling and molecular dynamics simulations. They propose that hIAPP channels consist of three to five oligomeric units assembled in the membrane (20). The ability of hIAPP oligomers to permeabilize the membrane has been demonstrated by the results of several studies conducted using unilamellar vesicles (LUV) or liposomal systems loaded with fluorescent calcein, and monitoring the fluorescence of the dye over time (8, 23). Furthermore, studies conducted on pancreatic β-cells by confocal microscopy show that the hIAPP oligomers were located near the cell membrane after two hours of incubation of the cells with the oligomers, while after four hours of incubation they were found in the cytoplasm. This result shows that oligomers can be internalized, thus causing cell death (8).

The aggregation rate of hIAPP depends on several factors, such as pH, peptide concentration, and metals. Several studies show that different metals are able to interact with the hIAPP molecule, modulating its secondary structure and subsequently the peptide's capacity to aggregate. Zn^{2+} (33, 37, 38), Al^{3+} (40) Au^{3+} (54) and Cu^{2+} (43) promote or inhibit fibril or aggregate formation, depending on metal concentration and different stages of the aggregation process. Therefore, all factors (including metal ions) that promote or inhibit the aggregation process consequently increase or decrease the cytotoxicity of the peptide.

Some metals are known environmental contaminants that penetrate our body and are deposited in various organs or systems. In particular, mercury and cadmium are two widespread environmental contaminants that are ingested or inhaled and accumulate in the central nervous system (CNS), liver and kidneys. Recent studies in animal systems have shown that these two metals can cause pancreatic cell dysfunction and apoptosis. The mechanisms underlying their effect have not yet been elucidated. The main aim of our work was to evaluate the effect of mercury and cadmium on the aggregation process of hIAPP by means of different techniques. The electrophysiological technique of measuring

the single channel current, although indirectly, provides information on the state of aggregation of the peptide, unlike electron microscopy and ThT assays which provide direct information.

The results obtained with the electrophysiological technique show that the central conductance and radius values of the hIAPP channel without pre-incubation are significantly higher than those with pre-incubation with Hg^{2+} or Cd^{2+}. Whereas the size of an ion channel depends on the number of peptide molecules that assemble into the membrane, our results seem to indicate that the number of subunits that assemble to form the conductive unit is lower when hIAPP is pre-incubated with the metal ions.

On the other hand, the frequency values of the hIAPP channel obtained by pre-incubating the peptide with mercury (regardless of the concentration used in this study) are significantly higher than those obtained with the peptide alone and through pre-incubation with cadmium. This result seems to indicate that, in solution, Hg^{2+} promotes the presence of hIAPP molecules prone to incorporate into the membrane and to form conductive units. Contrary to what was observed for mercury pre-incubation, Cd^{2+} appears to lower the hIAPP channel occurrence frequency in a concentration-dependent manner when used in pre-incubation. On increasing the cadmium concentration, the frequency values decrease compared to those obtained with the peptide alone. This result seems to indicate that Cd^{2+} favours the formation of stable aggregates in solution, which decrease the number of hIAPP molecules able to interact with the membrane. Several studies show that metal ions are able to bind to specific amino acid residues of the primary structure of human amylin. Specifically, the amino acids involved in binding with metal ions are His18 and Lys1. The studies by Loboda et al. and Rowinska-Zyrek (102, 103) report that the Zn^{2+} ion binds to the imidazole ring of His18 and to the amino group of Lys1. Patel and colleagues showed that the Zn^{2+} ion predominantly adopts a tetrahedral coordination geometry in forming a complex with proteins (37). It has been proven that Zn-imidazole binding is stronger in the Zn-hIAPP (1-37) complex than in the Zn-hIAPP (1-19) complex. Since the hIAPP peptide has only a single histidine, Zn^{2+} may coordinate three or four hIAPP peptide molecules, promoting the formation of large aggregates (38). Besides, Ramamoorthy's group has demonstrated that Zn^{2+} ions have different effects on hIAPP aggregation, depending on their concentration and the different stages of the amylin aggregation process itself (38). Unlike the Zn^{2+} ion, the Cu^{2+} ion appears to inhibit the formation of large aggregates and fibrils by stabilizing the hIAPP peptide in its native form (43-45). Cu^{2+} may bind to two amino acid sites in full-length hIAPP, one of those sites being Ala25 that is known for its importance in the misfolding of amylin, while the other binding site is positioned between residues 32 and 37 (104). The results obtained by Sinopoli and colleagues show an equilibrium between two conformations of hIAPP, with the more flexible state being the most dominant (data obtained with the MS technique) and random coil

conformation (data obtained with CD) in the presence of Cu^{2+} (46, 105). The inhibiting effect of Cu^{2+} on the fibril formation process may be due to the binding stoichiometry of hIAPP-Cu^{2+} that has a 1:1 ratio, even when the Cu^{2+} concentration is 20 times higher than that of the peptide, as found by Li et al. (43).

In light of these results and as we are not aware of similar studies with mercury and cadmium, we propose that the results obtained from the single channel experiments indicate, albeit indirectly, the different effect of Hg^{2+} and Cd^{2+} on the aggregation process of peptide in solution. We hypothesize that cadmium over the 24-hour incubation time (used in our study) promotes the aggregation process by shifting the monomer/aggregate reaction towards the formation of aggregates, which are unable to penetrate the membrane. By contrast, mercury promotes equilibrium of the monomer/aggregate reaction by making a greater number of peptide molecules available to interact with the membrane.

To test this hypothesis, we measured the ThT fluorescence intensity changes using the techniques of fluorescence spectroscopy and microscopy. Kinetic traces of ThT fluorescence were monitored in the absence and in the presence of different concentrations of Hg^{2+} or Cd^{2+}. The kinetic trend of the fluorescence of the fluorophore shows a significant decrease in intensity compared to that of the peptide alone when it is mixed with Hg^{2+}, regardless of the concentration of the ion used. Several studies show that the fluorescence intensity of ThT can be affected by changes in the binding constant and the quantum yield of ThT (106, 107). The fluorescence quantum yield depends not only on the ultra-fast oscillations of the ThT fragments in the excited state but also on the molecular configuration in the ground state. Therefore the quantum yield of ThT incorporated in amyloid aggregates depends on its conformation (107). The binding constant depends on the binding modes and sites of the amyloid aggregates (106). Since the amyloid aggregates formed by a peptide under different experimental conditions are not structurally identical (108, 109), it follows that the fluorescence intensity of bound ThT could be significantly different. Conversely, when the peptide is mixed with Cd^{2+}, the kinetic traces of ThT fluorescence show a significant increase in intensity compared to that in the absence of the ion.

These results seem to suggest that Cd^{2+} increases the level of amyloid aggregates while Hg^{2+} decreases it. Similar effects were also observed by fluorescence microscopy.

Numerous studies have shown that the aggregation process of hIAPP, as well as of other amyloid peptides, follows a nucleation-dependent polymerization process (21, 110). During primary or homogeneous nucleation, hIAPP monomers associate to form oligomers of various sizes, which constitute the critical nuclei. During heterogeneous nucleation, also called elongation, the reaction of critical nuclei with monomers enters a growth phase, characterized by the formation of high-molecular-weight aggregates, protofibrils and even the formation of mature fibrils. Finally, the

reaction reaches a steady state, in which the quantity of fibrils remains constant and in equilibrium with the previous species.

The nucleation-dependent polymerization process follows a sigmoidal kinetic trend in which the lag phase (corresponding to homogeneous nucleation) is a critical step that conditions the overall kinetics of the reaction. The duration of the lag phase can be influenced by various factors such as peptide concentration, temperature, pH, and ionic strength, purity (111).

The results of analyzing the TEM images obtained under the experimental conditions used in this work show that larger amyloid aggregates coexist with smaller aggregates, which tend to decrease in quantity over time according to the course of nucleation kinetics. TEM images obtained by pre-incubating the peptide with Hg^{2+} show both less electron-dense aggregates and a greater number of small aggregates than the images obtained by pre-incubating the peptide with Cd^{2+}, indicating the different effect of the two metals on the morphology of the aggregates. These results appear to be in agreement with those obtained with the other techniques used herein.

In conclusion, the results of our work show that: - hIAPP without and with pre-incubation with Hg^{2+} and Cd^{2+} forms ion channels in POPC PLMs, strengthening the concept that the cell membrane is the main target of hIAPP and suggesting a possible mechanism of toxicity; - Hg^{2+} and Cd^{2+} exert a different effect on the peptide molecules in solution suggesting a different mechanism of toxicity. Mercury, disfavouring the aggregation of peptide molecules in solution, promotes the formation of ion channels that can give rise to dysionia leading even to cellular dysfunction. Unlike mercury, cadmium promotes the formation of insoluble amyloid aggregates that could lead to apoptosis or cell mass reduction.

In light of these results, further studies will be conducted to evaluate the cytotoxicity of the amyloid aggregates shown in this study.

Acknowledgments

The authors acknowledge Anthony Green for proofreading and providing linguistic advice.

References

1. Fineman M, Weyer C, Maggs DG, Strobel S, Kolterman OG. The human amylin analog, pramlintide, reduces postprandial hyperglucagonemia in patients with type 2 diabetes mellitus. Horm Metab Res. 2002;34(9):504-8.
2. Weyer C, Maggs DG, Young AA, Kolterman OG. Amylin replacement with pramlintide as an adjunct to insulin therapy in type 1 and type 2 diabetes mellitus: a physiological approach toward improved metabolic control. Curr Pharm Des. 2001;7(14):1353-73.
3. Akesson B, Panagiotidis G, Westermark P, Lundquist I. Islet amyloid polypeptide inhibits glucagon release and exerts a dual action on insulin release from isolated islets. Regul Pept. 2003;111(1-3):55-60.
4. Reda TK, Geliebter A, Pi-Sunyer FX. Amylin, food intake, and obesity. Obes Res. 2002;10(10):1087-91.
5. Westermark P, Wernstedt C, Wilander E, Sletten K. A novel peptide in the calcitonin gene related peptide family as an amyloid fibril protein in the endocrine pancreas. Biochem Biophys Res Commun. 1986;140(3):827-31.
6. Hartl FU. Protein Misfolding Diseases. Annu Rev Biochem. 2017;86:21-6.
7. Ivanova MI, Lin Y, Lee YH, Zheng J, Ramamoorthy A. Biophysical processes underlying cross-seeding in amyloid aggregation and implications in amyloid pathology. Biophys Chem. 2021;269:106507.
8. Bram Y, Frydman-Marom A, Yanai I, Gilead S, Shaltiel-Karyo R, Amdursky N, et al. Apoptosis induced by islet amyloid polypeptide soluble oligomers is neutralized by diabetes-associated specific antibodies. Sci Rep. 2014;4:4267.
9. Milardi D, Gazit E, Radford SE, Xu Y, Gallardo RU, Caflisch A, et al. Proteostasis of Islet Amyloid Polypeptide: A Molecular Perspective of Risk Factors and Protective Strategies for Type II Diabetes. Chem Rev. 2021;121(3):1845-93.
10. Röcken C, Linke RP, Saeger W. Immunohistology of islet amyloid polypeptide in diabetes mellitus: Semi-qantitative studies in a post-mortem series. Virchows Archiv A. 1992;421:339-44.
11. Sakagashira S, Hiddinga HJ, Tateishi K, Sanke T, Hanabusa T, Nanjo K, et al. S20G mutant amylin exhibits increased in vitro amyloidogenicity and increased intracellular cytotoxicity compared to wild-type amylin. Am J Pathol. 2000;157(6):2101-9.
12. Luca S, Yau WM, Leapman R, Tycko R. Peptide conformation and supramolecular organization in amylin fibrils: constraints from solid-state NMR. Biochemistry. 2007;46(47):13505-22.
13. Quist A, Doudevski I, Lin H, Azimova R, Ng D, Frangione B, et al. Amyloid ion channels: a common structural link for protein-misfolding disease. Proc Natl Acad Sci U S A. 2005;102(30):10427-32.
14. Zhao J, Yu X, Liang G, Zheng J. Heterogeneous triangular structures of human islet amyloid polypeptide (amylin) with internal hydrophobic cavity and external wrapping morphology reveal the polymorphic nature of amyloid fibrils. Biomacromolecules. 2011;12(5):1781-94.
15. Zhao J, Yu X, Liang G, Zheng J. Structural polymorphism of human islet amyloid polypeptide (hIAPP) oligomers highlights the importance of interfacial residue interactions. Biomacromolecules. 2011;12(1):210-20.
16. Nguyen PH, Ramamoorthy A, Sahoo BR, Zheng J, Faller P, Straub JE, et al. Amyloid Oligomers: A Joint Experimental/Computational Perspective on Alzheimer's Disease, Parkinson's Disease, Type II Diabetes, and Amyotrophic Lateral Sclerosis. Chem Rev. 2021;121(4):2545-647.
17. Poyner DR, Sexton PM, Marshall I, Smith DM, Quirion R, Born W, et al. International Union of Pharmacology. XXXII. The mammalian calcitonin gene-related peptides, adrenomedullin, amylin, and calcitonin receptors. Pharmacol Rev. 2002;54(2):233-46.
18. Christopoulos G, Perry KJ, Morfis M, Tilakaratne N, Gao Y, Fraser NJ, et al. Multiple amylin receptors arise from receptor activity-modifying protein interaction with the calcitonin receptor gene product. Mol Pharmacol. 1999;56(1):235-42.

19. Jhamandas JH, Mactavish D. β-Amyloid protein (Aβ) and human amylin regulation of apoptotic genes occurs through the amylin receptor. Apoptosis. 2012;17(1):37-47.
20. Zhao J, Luo Y, Jang H, Yu X, Wei G, Nussinov R, et al. Probing ion channel activity of human islet amyloid polypeptide (amylin). Biochim Biophys Acta. 2012;1818(12):3121-30.
21. Caillon L, Hoffmann AR, Botz A, Khemtemourian L. Molecular Structure, Membrane Interactions, and Toxicity of the Islet Amyloid Polypeptide in Type 2 Diabetes Mellitus. J Diabetes Res. 2016;2016:5639875.
22. Dong X, Qiao Q, Qian Z, Wei G. Recent computational studies of membrane interaction and disruption of human islet amyloid polypeptide: Monomers, oligomers and protofibrils. Biochim Biophys Acta Biomembr. 2018;1860(9):1826-39.
23. Zhang X, St Clair JR, London E, Raleigh DP. Islet Amyloid Polypeptide Membrane Interactions: Effects of Membrane Composition. Biochemistry. 2017;56(2):376-90.
24. Jayasinghe SA, Langen R. Membrane interaction of islet amyloid polypeptide. Biochim Biophys Acta. 2007;1768(8):2002-9.
25. Qian Z, Zou Y, Zhang Q, Chen P, Ma B, Wei G, et al. Atomistic-level study of the interactions between hIAPP protofibrils and membranes: Influence of pH and lipid composition. Biochim Biophys Acta Biomembr. 2018;1860(9):1818-25.
26. Jia Y, Qian Z, Zhang Y, Wei G. Adsorption and Orientation of Human Islet Amyloid Polypeptide (hIAPP) Monomer at Anionic Lipid Bilayers: Implications for Membrane-Mediated Aggregation. Int J Mol Sci. 2013;14(3):6241-58.
27. Sparr E, Engel MF, Sakharov DV, Sprong M, Jacobs J, de Kruijff B, et al. Islet amyloid polypeptide-induced membrane leakage involves uptake of lipids by forming amyloid fibers. FEBS Lett. 2004;577(1-2):117-20.
28. Khemtémourian L, Engel MF, Kruijtzer JA, Höppener JW, Liskamp RM, Killian JA. The role of the disulfide bond in the interaction of islet amyloid polypeptide with membranes. Eur Biophys J. 2010;39(9):1359-64.
29. Jha S, Snell JM, Sheftic SR, Patil SM, Daniels SB, Kolling FW, et al. pH dependence of amylin fibrillization. Biochemistry. 2014;53(2):300-10.
30. Khemtémourian L, Doménech E, Doux JP, Koorengevel MC, Killian JA. Low pH acts as inhibitor of membrane damage induced by human islet amyloid polypeptide. J Am Chem Soc. 2011;133(39):15598-604.
31. Poulson BG, Szczepski K, Lachowicz JI, Jaremko L, Abdul-Hamid E, Jaremko M. Aggregation of biologically important peptides and proteins: inhibition or accelerationdepending on protein and metal ion concentrations. RSC Adv. 2020;10:215-27.
32. Beck Erlach M, Kalbitzer HR, Winter R, Kremer W. The pressure and temperature perturbation approach reveals a whole variety of conformational substates of amyloidogenic hIAPP monitored by 2D NMR spectroscopy. Biophys Chem. 2019;254:106239.
33. Brender JR, Hartman K, Nanga RP, Popovych N, de la Salud Bea R, Vivekanandan S, et al. Role of zinc in human islet amyloid polypeptide aggregation. J Am Chem Soc. 2010;132(26):8973-83.
34. Khemtemourian L, Antoniciello F, Sahoo BR, Decossas M, Lecomte S, Ramamoorthy A. Investigation of the effects of two major secretory granules components, insulin and zinc, on human-IAPP amyloid aggregation and membrane damage. Chem Phys Lipids. 2021;237:105083.
35. Magzoub M, Miranker AD. Concentration-dependent transitions govern the subcellular localization of islet amyloid polypeptide. FASEB J. 2012;26(3):1228-38.
36. Casey JR, Grinstein S, Orlowski J. Sensors and regulators of intracellular pH. Nat Rev Mol Cell Biol. 2010;11(1):50-61.
37. Patel K, Kumar A, Durani S. Analysis of the structural consensus of the zinc coordination centers of metalloprotein structures. Biochim Biophys Acta. 2007;1774(10):1247-53.

38. Brender JR, Krishnamoorthy J, Messina GM, Deb A, Vivekanandan S, La Rosa C, et al. Zinc stabilization of prefibrillar oligomers of human islet amyloid polypeptide. Chem Commun (Camb). 2013;49(32):3339-41.
39. Salamekh S, Brender JR, Hyung SJ, Nanga RP, Vivekanandan S, Ruotolo BT, et al. A two-site mechanism for the inhibition of IAPP amyloidogenesis by zinc. J Mol Biol. 2011;410(2):294-306.
40. Ward B, Walker K, Exley C. Copper(II) inhibits the formation of amylin amyloid in vitro. J Inorg Biochem. 2008;102(2):371-5.
41. Mold M, Bunrat C, Goswami P, Roberts A, Roberts C, Taylor N, et al. Further insight into the role of metals in amyloid formation by IAPP1-37 and ProIAPP1-48. Journal of Diabetes Research & Clinical Metabolism 2015;4(4).
42. Ge X, Kakinen A, Gurzov EN, Yang W, Pang L, Pilkington EH, et al. Zinc-coordination and C-peptide complexation: a potential mechanism for the endogenous inhibition of IAPP aggregation. Chem Commun (Camb). 2017;53(68):9394-7.
43. Li H, Ha E, Donaldson RP, Jeremic AM, Vertes A. Rapid assessment of human amylin aggregation and its inhibition by copper(II) ions by laser ablation electrospray ionization mass spectrometry with ion mobility separation. Anal Chem. 2015;87(19):9829-37.
44. Lee EC, Ha E, Singh S, Legesse L, Ahmad S, Karnaukhova E, et al. Copper(II)-human amylin complex protects pancreatic cells from amylin toxicity. Phys Chem Chem Phys. 2013;15(30):12558-71.
45. Mirhashemi SM, Shahabaddin ME. Evaluation of aluminium, manganese, copper and selenium effects on human islets amyloid polypeptide hormone aggregation. Pak J Biol Sci. 2011;14(4):288-92.
46. Sinopoli A, Magrì A, Milardi D, Pappalardo M, Pucci P, Flagiello A, et al. The role of copper(II) in the aggregation of human amylin. Metallomics. 2014;6(10):1841-52.
47. Mukherjee S, Dey SG. Heme bound amylin: spectroscopic characterization, reactivity, and relevance to type 2 diabetes. Inorg Chem. 2013;52(9):5226-35.
48. He L, Wang X, Zhao C, Wang H, Du W. Ruthenium complexes as novel inhibitors of human islet amyloid polypeptide fibril formation. Metallomics. 2013;5(12):1599-603.
49. Zhu D, Gong G, Wang W, Du W. Disaggregation of human islet amyloid polypeptide fibril formation by ruthenium polypyridyl complexes. J Inorg Biochem. 2017;170:109-16.
50. Gong G, Wang W, Du W. Binuclear ruthenium complexes inhibit the fibril formation of human islet amyloid polypeptide. RSC Adv. 2017;7:18512-22.
51. Ma L, Fu Y, Yu L, Li X, Zheng W, Chen T. Ruthenium complexes as inhibitors of human islet amyloid polypeptide aggregation, an effect that prevents beta cell apoptosis. RSC Adv. 2015;5:17405-12.
52. He L, Wang X, Zhao C, Zhu D, Du W. Inhibition of human amylin fibril formation by insulin-mimetic vanadium complexes. Metallomics. 2014;6(5):1087-96.
53. Niu X, Xiao R, Wang N, Wang Z, Zhang Y, Xia Q, et al. The Molecular Mechanisms and Rational Design of Anti-Diabetic Vanadium Compounds. Curr Top Med Chem. 2016;16(8):811-22.
54. He L, Zhu D, Zhao C, Jia X, Wang X, Du W. Effects of gold complexes on the assembly behavior of human islet amyloid polypeptide. J Inorg Biochem. 2015;152:114-22.
55. Chen L, Lei L, Jin T, Nordberg M, Nordberg GF. Plasma metallothionein antibody, urinary cadmium, and renal dysfunction in a Chinese type 2 diabetic population. Diabetes Care. 2006;29(12):2682-7.
56. Xiao L, Li W, Zhu C, Yang S, Zhou M, Wang B, et al. Cadmium exposure, fasting blood glucose changes, and type 2 diabetes mellitus: A longitudinal prospective study in China. Environ Res. 2021;192:110259.
57. Kolachi NF, Kazi TG, Afridi HI, Kazi N, Khan S, Kandhro GA, et al. Status of toxic metals in biological samples of diabetic mothers and their neonates. Biol Trace Elem Res. 2011;143(1):196-212.

58. Afridi HI, Kazi TG, Kazi N, Jamali MK, Arain MB, Jalbani N, et al. Evaluation of status of toxic metals in biological samples of diabetes mellitus patients. Diabetes Res Clin Pract. 2008;80(2):280-8.
59. Schwartz GG, Il'yasova D, Ivanova A. Urinary cadmium, impaired fasting glucose, and diabetes in the NHANES III. Diabetes Care. 2003;26(2):468-70.
60. Wallia A, Allen NB, Badon S, El Muayed M. Association between urinary cadmium levels and prediabetes in the NHANES 2005-2010 population. Int J Hyg Environ Health. 2014;217(8):854-60.
61. Haswell-Elkins M, Satarug S, O'Rourke P, Moore M, Ng J, McGrath V, et al. Striking association between urinary cadmium level and albuminuria among Torres Strait Islander people with diabetes. Environ Res. 2008;106(3):379-83.
62. Little BB, Reilly R, Walsh B, Vu GT. Cadmium Is Associated with Type 2 Diabetes in a Superfund Site Lead Smelter Community in Dallas, Texas. Int J Environ Res Public Health. 2020;17(12).
63. Roy C, Tremblay PY, Ayotte P. Is mercury exposure causing diabetes, metabolic syndrome and insulin resistance? A systematic review of the literature. Environ Res. 2017;156:747-60.
64. Dufault R, Berg Z, Crider R, Schnoll R, Wetsit L, Bulls WT, et al. Blood inorganic mercury is directly associated with glucose levels in the human population and may be linked to processed food intake. Integr Mol Med. 2015;2(3).
65. He K, Xun P, Liu K, Morris S, Reis J, Guallar E. Mercury exposure in young adulthood and incidence of diabetes later in life: the CARDIA Trace Element Study. Diabetes Care. 2013;36(6):1584-9.
66. Cordier S, Anassour-Laouan-Sidi E, Lemire M, Costet N, Lucas M, Ayotte P. Association between exposure to persistent organic pollutants and mercury, and glucose metabolism in two Canadian Indigenous populations. Environ Res. 2020;184:109345.
67. Jeppesen C, Valera B, Nielsen NO, Bjerregaard P, Jørgensen ME. Association between whole blood mercury and glucose intolerance among adult Inuit in Greenland. Environ Res. 2015;143(Pt A):192-7.
68. El Muayed M, Raja MR, Zhang X, MacRenaris KW, Bhatt S, Chen X, et al. Accumulation of cadmium in insulin-producing β cells. Islets. 2012;4(6):405-16.
69. Fitzgerald R, Olsen A, Nguyen J, Wong W, El Muayed M, Edwards J. Pancreatic Islets Accumulate Cadmium in a Rodent Model of Cadmium-Induced Hyperglycemia. Int J Mol Sci. 2021;22(1).
70. Han JC, Park SY, Hah BG, Choi GH, Kim YK, Kwon TH, et al. Cadmium induces impaired glucose tolerance in rat by down-regulating GLUT4 expression in adipocytes. Arch Biochem Biophys. 2003;413(2):213-20.
71. Chen YW, Huang CF, Yang CY, Yen CC, Tsai KS, Liu SH. Inorganic mercury causes pancreatic beta-cell death via the oxidative stress-induced apoptotic and necrotic pathways. Toxicol Appl Pharmacol. 2010;243(3):323-31.
72. Schumacher L, Abbott LC. Effects of methyl mercury exposure on pancreatic beta cell development and function. J Appl Toxicol. 2017;37(1):4-12.
73. Chen K-L, Liu S-H, Su C-C, Yen C-C, Yang C-Y, Lee K-I, et al. Mercuric Compounds Induce Pancreatic Islets Dysfunction and Apoptosis in Vivo. Int J Mol Sci. 2012;13:12349-66.
74. Lenzen S. Oxidative stress: the vulnerable beta-cell. Biochem Soc Trans. 2008;36(Pt 3):343-7.
75. Yang TY, Xu ZF, Liu W, Xu B, Deng Y, Li YH, et al. Alpha-lipoic acid protects against methylmercury-induced neurotoxic effects via inhibition of oxidative stress in rat cerebral cortex. Environ Toxicol Pharmacol. 2015;39(1):157-66.
76. Caito SW, Aschner M. Mitochondrial Redox Dysfunction and Environmental Exposures. Antioxid Redox Signal. 2015;23(6):578-95.

77. Rolo AP, Palmeira CM. Diabetes and mitochondrial function: role of hyperglycemia and oxidative stress. Toxicol Appl Pharmacol. 2006;212(2):167-78.
78. Mozaffarian D, Shi P, Morris JS, Grandjean P, Siscovick DS, Spiegelman D, et al. Methylmercury exposure and incident diabetes in U.S. men and women in two prospective cohorts. Diabetes Care. 2013;36(11):3578-84.
79. Barregard L, Bergström G, Fagerberg B. Cadmium exposure in relation to insulin production, insulin sensitivity and type 2 diabetes: a cross-sectional and prospective study in women. Environ Res. 2013;121:104-9.
80. Borné Y, Fagerberg B, Persson M, Sallsten G, Forsgard N, Hedblad B, et al. Cadmium exposure and incidence of diabetes mellitus--results from the Malmö Diet and Cancer study. PLoS One. 2014;9(11):e112277.
81. Moon S-S. Association of lead, mercury and cadmium with diabetes in the Korean population: The Korea National Health and Nutrition Examination Survey (KNHANES) 2009–2010. Diabet Med. 2013;30(4):e143-e8.
82. Nordberg GF, Bernarda A, Diamond GL, Duffus JH, Illing P, Nordberg M, et al. Risk assessment of effects of cadmium on human health (IUPAC Technical Report). Pure Appl Chem. 2018;90(4):755-808.
83. Micelli S, Meleleo D, Picciarelli V, Gallucci E. Effect of sterols on beta-amyloid peptide (AbetaP 1-40) channel formation and their properties in planar lipid membranes. Biophys J. 2004;86(4):2231-7.
84. Ciardiello MA, Meleleo D, Saviano G, Crescenzo R, Carratore V, Camardella L, et al. Kissper, a kiwi fruit peptide with channel-like activity: structural and functional features. J Pept Sci. 2008;14(6):742-54.
85. Meleleo D, Galliani A, Notarachille G. AβP1-42 incorporation and channel formation in planar lipid membranes: the role of cholesterol and its oxidation products. J Bioenerg Biomembr. 2013;45(4):369-81.
86. Notarachille G, Gallucci E, Micelli S, Meleleo D. Effect of cadmium ions on amyloid beta peptide 1-42 channel activity. Journal of Environmental Chemistry and Ecotoxicology. 2011;3(12):309-19.
87. Meleleo D, Notarachille G, Mangini V, Arnesano F. Concentration-dependent effects of mercury and lead on Aβ42: possible implications for Alzheimer's disease. Eur Biophys J. 2019;48(2):173-87.
88. Müller P, Rudin D, Tien T, Weacott W. Reconstitution of cell membrane structure in vitro and its trasformation into an excitable system. Nature. 1962;194:979-80.
89. Tien, H. T. Bilayer Lipid Membrane: Theory and Practice. New York: Marcel Dekker; 1974.
90. Tien T, Mountz J, Martinosi A. Protein-lipid interaction in bilayer lipid membranes (BLM). The Enzyme of Biological Membranes. NY Plenum1977. p. 139-70.
91. Gallucci E, Meleleo D, Micelli S, Picciarelli V. Magainin 2 channel formation in planar lipid membranes: the role of lipid polar groups and ergosterol. Eur Biophys J. 2003;32(1):22-32.
92. Stipani V, Gallucci E, Micelli S, Picciarelli V, Benz R. Channel formation by salmon and human calcitonin in black lipid membranes. Biophys J. 2001;81(6):3332-8.
93. Micelli S, Gallucci E, Meleleo D, Stipani V, Picciarelli V. Mitochondrial porin incorporation into black lipid membranes: ionic and gating contribution to the total current. Bioelectrochemistry. 2002;57(2):97-106.
94. Arispe N, Pollard H, Rojas E. Zn2+ interaction with Alzheimer amyloid beta protein calcium channels. Proc Natl Acad Sci U S A. 1996;93(4):1710-5.
95. Lorenzo A, Razzaboni B, Weir GC, Yankner BA. Pancreatic islet cell toxicity of amylin associated with type-2 diabetes mellitus. Nature. 1994;368(6473):756-60.
96. Mirzabekov TA, Lin MC, Kagan BL. Pore formation by the cytotoxic islet amyloid peptide amylin. J Biol Chem. 1996;271(4):1988-92.

97. Sciacca MF, Kotler SA, Brender JR, Chen J, Lee DK, Ramamoorthy A. Two-step mechanism of membrane disruption by Aβ through membrane fragmentation and pore formation. Biophys J. 2012;103(4):702-10.
98. Sciacca MF, Brender JR, Lee DK, Ramamoorthy A. Phosphatidylethanolamine enhances amyloid fiber-dependent membrane fragmentation. Biochemistry. 2012;51(39):7676-84.
99. Sciacca MF, Pappalardo M, Milardi D, Grasso DM, La Rosa C. Calcium-activated membrane interaction of the islet amyloid polypeptide: implications in the pathogenesis of type II diabetes mellitus. Arch Biochem Biophys. 2008;477(2):291-8.
100. Sciacca MF, Milardi D, Messina GM, Marletta G, Brender JR, Ramamoorthy A, et al. Cations as switches of amyloid-mediated membrane disruption mechanisms: calcium and IAPP. Biophys J. 2013;104(1):173-84.
101. Milardi D, Sciacca MF, Randazzo L, Raudino A, La Rosa C. The role of calcium, lipid membranes and islet amyloid polypeptide in the onset of type 2 diabetes: innocent bystanders or partners in a crime? Front Endocrinol (Lausanne). 2014;5:216.
102. Łoboda D, Rowińska-Żyrek M. Zn(II) - pramlintide: Stability, binding sites and unexpected aggregation. J Inorg Biochem. 2017;174:150-5.
103. Rowińska-Żyrek M. Coordination of Zn(2+) and Cu(2+) to the membrane disrupting fragment of amylin. Dalton Trans. 2016;45(19):8099-106.
104. Riba I, Barran PE, Cooper GJS, Unwin RD. On the structure of the copper–amylin complex. Int J Mass Spectrom. 2015;391:47-53.
105. Sánchez-López C, Cortés-Mejía R, Miotto MC, Binolfi A, Fernández CO, Del Campo JM, et al. Copper Coordination Features of Human Islet Amyloid Polypeptide: The Type 2 Diabetes Peptide. Inorg Chem. 2016;55(20):10727-40.
106. Sulatskaya AI, Kuznetsova IM, Turoverov KK. Interaction of thioflavin T with amyloid fibrils: stoichiometry and affinity of dye binding, absorption spectra of bound dye. J Phys Chem B. 2011;115(39):11519-24.
107. Sulatskaya AI, Maskevich AA, Kuznetsova IM, Uversky VN, Turoverov KK. Fluorescence quantum yield of thioflavin T in rigid isotropic solution and incorporated into the amyloid fibrils. PLoS One. 2010;5(10):e15385.
108. Biancalana M, Koide S. Molecular mechanism of Thioflavin-T binding to amyloid fibrils. Biochim Biophys Acta. 2010;1804(7):1405-12.
109. Loksztejn A, Dzwolak W. Chiral bifurcation in aggregating insulin: an induced circular dichroism study. J Mol Biol. 2008;379(1):9-16.
110. Asthana S, Mallick B, Alexandrescu AT, Jha S. IAPP in type II diabetes: Basic research on structure, molecular interactions, and disease mechanisms suggests potential intervention strategies. Biochim Biophys Acta Biomembr. 2018;1860(9):1765-82.
111. Lundqvist M, Rodriguez Camargo DC, Bernfur K, Chia S, Linse S. Expression, purification and characterisation of large quantities of recombinant human IAPP for mechanistic studies. Biophys Chem. 2021;269:106511.

Figure Legends

Figure 1 hIAPP channel activity without and with preincubation with $HgCl_2$ and $CdCl_2$ for 24 hours. Representative traces illustrating the channel activity of hIAPP in membranes made up of POPC. Channel activity was recorded after an average of 20 minutes from first channel formation, when channel activity is substantial and lasting. Applied voltage was set to 60 mV. Experimental conditions: KCl 0.1 M (pH 7) and T = 23±1°C.

Figure 2 Kinetics of hIAPP amyloid aggregate formation monitored by ThT fluorescence. (A) Amyloid aggregate formation ThT curves for 10 μM hIAPP alone (□) and with 10 μM Hg^{2+} (Δ) or Cd^{2+} (○). (B) Amyloid aggregate formation ThT curves for 10 μM hIAPP alone (□) and with 50 μM Hg^{2+} (Δ) or Cd^{2+} (○). Data points and error bars shown represent mean ± standard error of three experiments performed in duplicate. (C) Dose dependent ThT assay of hIAPP (10 μM) in absence (□) and presence of different concentrations of Hg^{2+} (Δ) and Cd^{2+} (○).Experimental conditions: T = 25°C, pH = 7.4.

Figure 3 ThT fluorescence microscopy images. Representative images show amyloid aggregates of 10 μM hIAPP alone (A, B, C) and with 50 μM Hg^{2+} (D, E, F) or Cd^{2+} (G, H, I) at time 0h (T0) and after 24h (T24) and 72h (T72) incubation at 25°C. Scale bar is 100 μm.

Figure 4 TEM images of hIAPP aggregates. Amyloid aggregates of 10 μM hIAPP alone (A,B,C), hIAPP preincubated with Hg^{2+} (D,E,F) or Cd^{2+} (G,H,I) 10 μM and Hg^{2+} (L,M,N) or Cd^{2+} (O,P,Q) 50 μM for 0h (T0), 24h (T24) and 72h (T72). Some examples of short and scattered aggregates are circled in red. Scale bar is 250 nm.

Table 1 Mean conductance of hIAPP channel without and with pre-incubation with different $HgCl_2$ and $CdCl_2$ concentrations for 24 hours. The central conductance ± standard error (Λ_c±SE) of the hIAPP channel pre-incubated with 0.1 and 0.5 μM of $HgCl_2$ and $CdCl_2$ in POPC PLMs. The minimum and maximum number of channels considered (N) out of a total number of channels considered (N_t) was: [hIAPP] =0.1 μM, 255<N<802, Nt=3868; [hIAPP+Hg^{2+}] =0.1 μM+0.1 μM, 253<N<1315, Nt=4399; [hIAPP+Cd^{2+}] =0.1 μM+0.1 μM, 221<N<596, Nt=2518; [hIAPP+Hg^{2+}] =0.1 μM+0.5 μM, 219<N<1295, Nt=4505; [hIAPP+Cd^{2+}] =0.1 μM+0.5 μM, 110<N<217, Nt=1120.

Table 2 Channel frequency of hIAPP without and with pre-incubation with different $HgCl_2$ and $CdCl_2$ concentrations for 24 hours. The frequency ± standard deviation (F±SD) of the hIAPP channel pre-incubated with 0.1 and 0.5 μM of $HgCl_2$ and $CdCl_2$ in POPC PLMs. The minimum and maximum number of channels considered (N) out of a total number of channels considered (N_t) is reported in the legend to Table 1.

Table 1

	[hIAPP] [0.1 μM]	[hIAPP+Hg^{2+}] [0.1 μM+0.1μM]	[hIAPP+Cd^{2+}] [0.1 μM+0.1μM]	[hIAPP+Hg^{2+}] [0.1 μM+0.5μM]	[hIAPP+Cd^{2+}] [0.1 μM+0.5μM]
Vs mV	Λc±SE nS	Λc±SE nS	Λc±SE nS	Λc±SE nS	Λc±SE nS
100	0.023±0.001	0.022±0.001	0.023±0.0008	0.027±0.001	0.025±0.0008
80	0.036±0.003	0.030±0.001	0.034±0.002	0.027±0.0006	0.033±0.002
60	0.062±0.002	0.043±0.002	0.045±0.002	0.033±0.001	0.037±0.002
40	0.077±0.004			0.055±0.002	0.046±0.004
20	0.199±0.008				
-20	0.108±0.010				
-40	0.083±0.003			0.043±0.002	0.041±0.007
-60	0.050±0.002	0.039±0.003	0.038±0.001	0.032±0.0008	0.034±0.001
-80	0.037±0.002	0.028±0.0007	0.020±0.001	0.029±0.0009	0.024±0.002
-100	0.028±0.001	0.018±0.001	0.020±0.0006	0.020±0.0005	0.020±0.0008

Table 2

	[hIAPP] [0.1 μM]	[hIAPP+Hg^{2+}] [0.1 μM+0.1μM]	[hIAPP+Cd^{2+}] [0.1 μM+0.1μM]	[hIAPP+Hg^{2+}] [0.1 μM+0.5μM]	[hIAPP+Cd^{2+}] [0.1 μM+0.5μM]
Vs mV	F±SD	F±SD	F±SD	F±SD	F±SD
100	5.77±0.28	8.90±0.33	5.11±0.41	13.36±0.69	1.57±0.10
80	5.34±0.19	8.86±0.24	6.15±0.25	10.78±0.35	1.92±0.17
60	5.04±0.26	14.66±0.49	5.07±0.39	8.96±0.30	3.49±0.33
40	3.85±0.32			10.52±0.42	3.02±0.41
20	6.69±0.90				
-20	6.55±1.81				
-40	3.27±0.40			6.97±0.39	2.52±0.35
-60	3.21±0.14	8.69±0.55	4.96±0.27	6.07±0.35	2.45±0.23
-80	5.90±0.25	9.60±0.38	2.71±0.17	7.33±0.40	2.01±0.12
-100	5.01±0.35	8.00±0.33	4.25±0.21	7.48±0.35	1.81±0.18

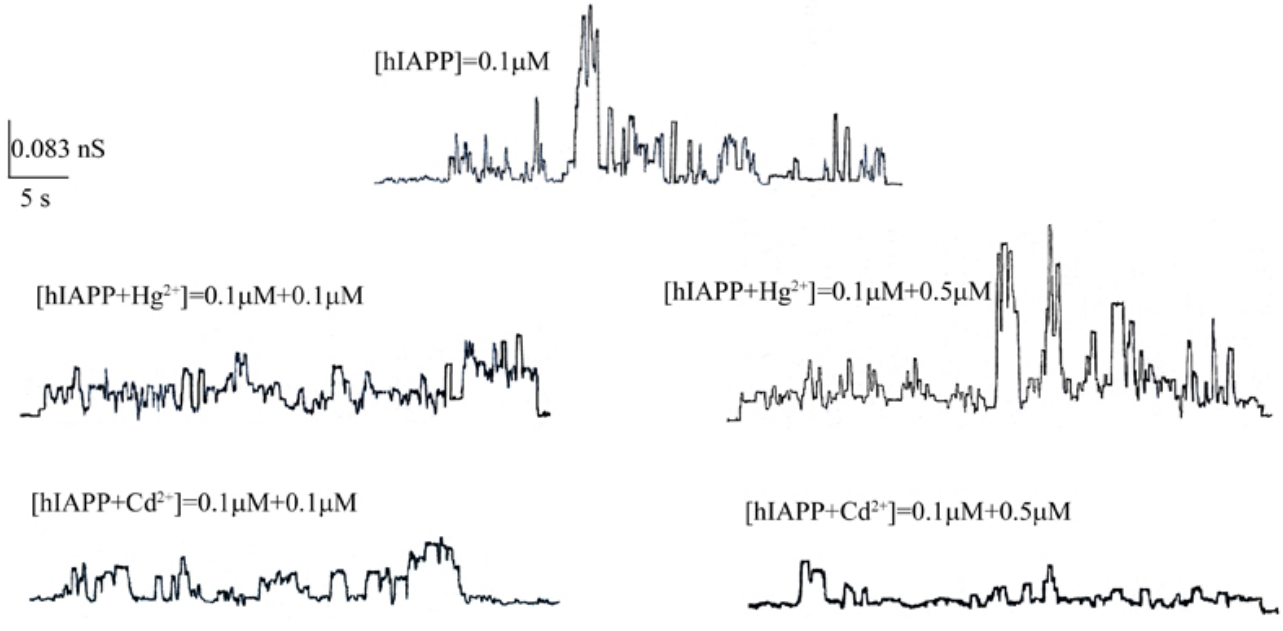
[hIAPP]=0.1μM
0.083 nS
5 s
[hIAPP+Hg2+]=0.1μM+0.1μM
[hIAPP+Hg2+]=0.1μM+0.5μM
[hIAPP+Cd2+]=0.1μM+0.1μM
[hIAPP+Cd2+]=0.1μM+0.5μM

Fig. 1

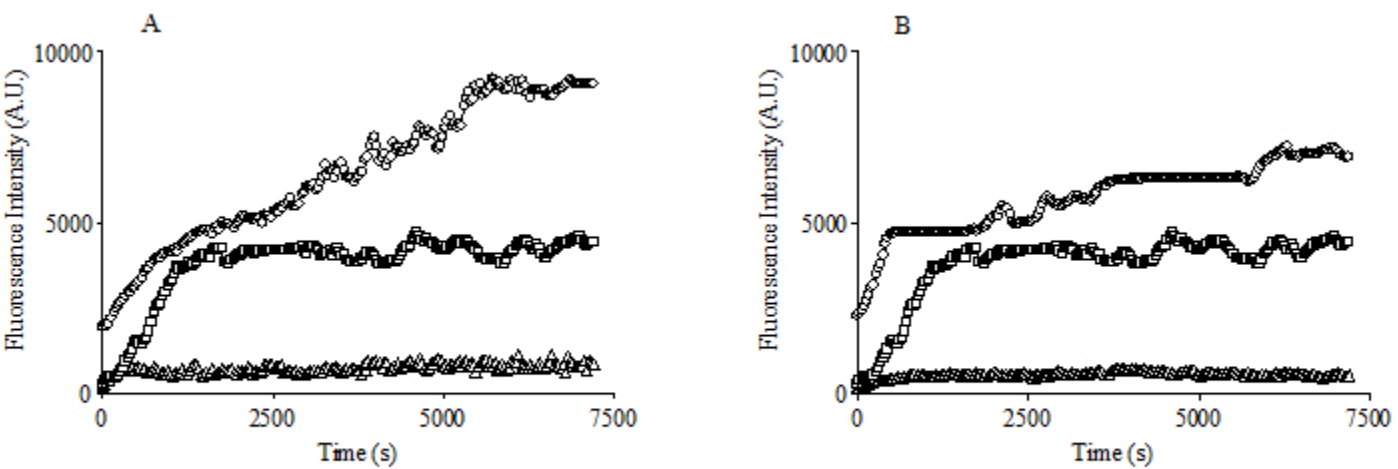
A
B
10000
5000
0
Fluorescence Intensity (A.U.)
0
2500
5000
7500
Time (s)

Fig. 2

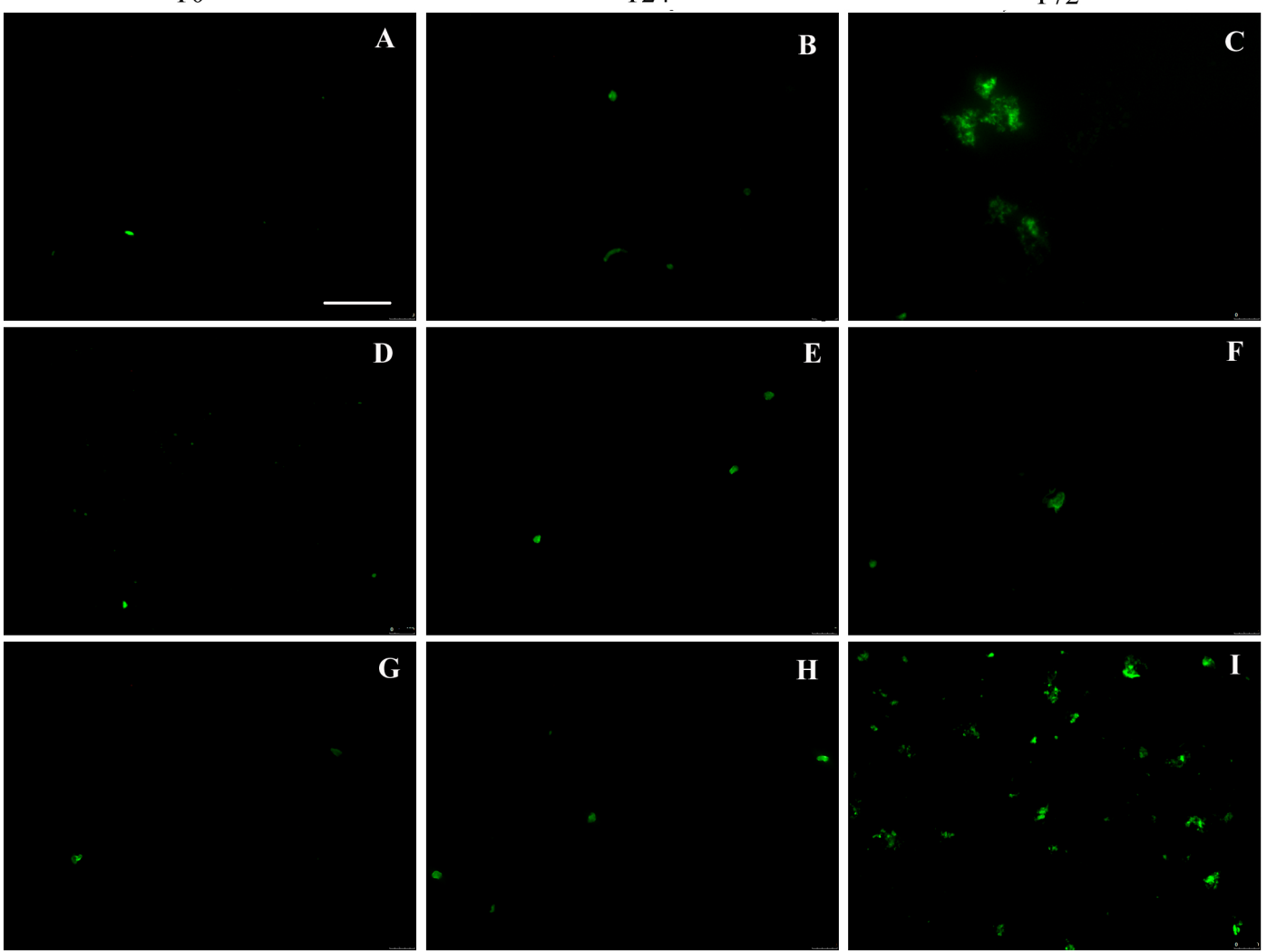

Fig.3

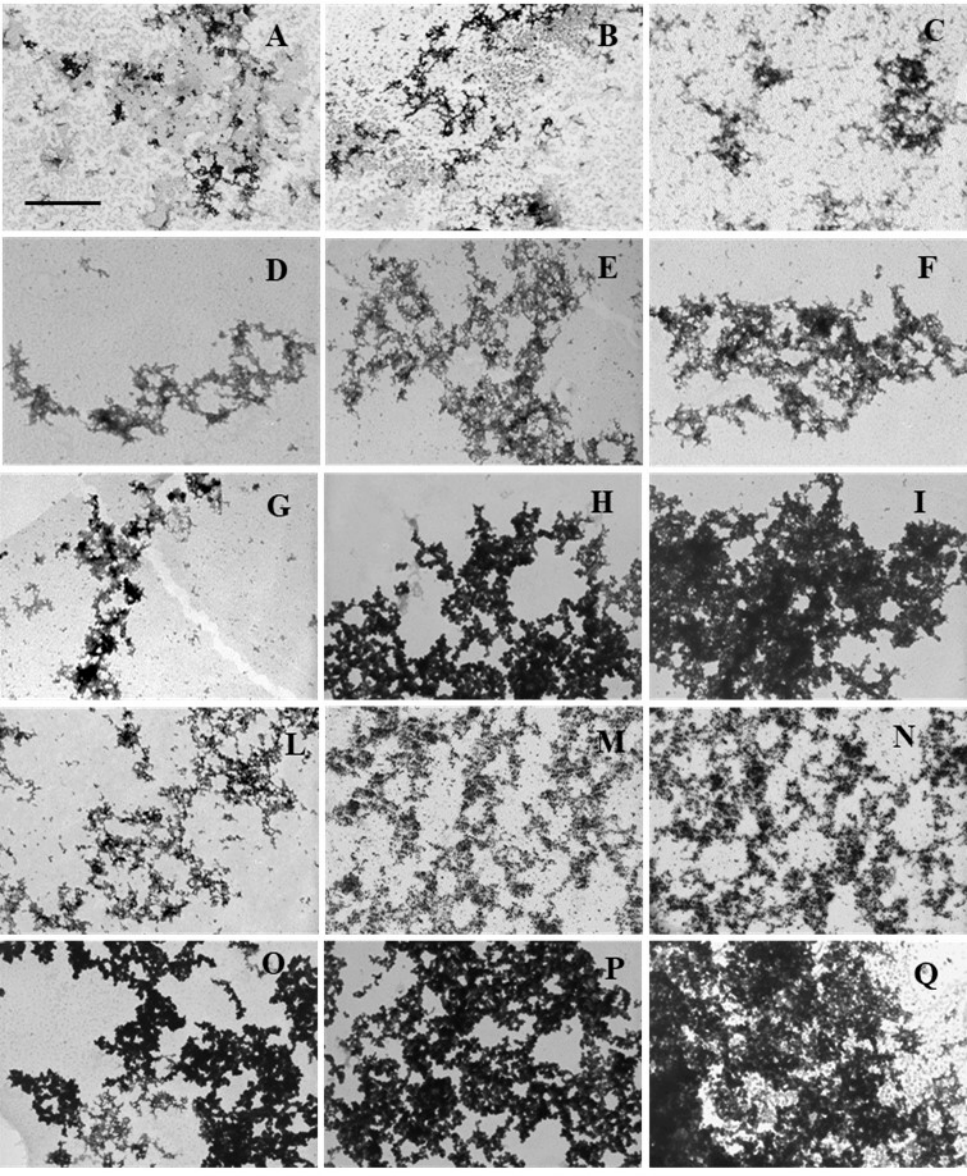

Fig. 4